Global Sensitivity Analysis of Bulk Properties of an Atomic Nucleus

Andreas Ekström[1] and Gaute Hagen[2,3]
[1]Department of Physics, Chalmers University of Technology, SE-412 96 Göteborg, Sweden
[2]Physics Division, Oak Ridge National Laboratory, Oak Ridge, Tennessee 37831, USA
[3]Department of Physics and Astronomy, University of Tennessee, Knoxville, Tennessee 37996, USA

(Received 10 October 2019; revised manuscript received 12 November 2019; published 20 December 2019)

We perform a global sensitivity analysis of the binding energy and the charge radius of the nucleus ^{16}O to identify the most influential low-energy constants in the next-to-next-to-leading order chiral Hamiltonian with two- and three-nucleon forces. For this purpose, we develop a subspace-projected coupled-cluster method using eigenvector continuation [Frame D. *et al.*, Phys. Rev. Lett. **121**, 032501 (2018)]. With this method, we compute the binding energy and charge radius of ^{16}O at more than 10^6 different values of the 16 low-energy constants in one hour on a standard laptop computer. For relatively small subspace projections, the root-mean-square error is about 1% compared to full-space coupled-cluster results. We find that 58(1)% of the variance in energy can be apportioned to a single contact term in the $^3S_1$ wave, whereas the radius depends sensitively on several low-energy constants and their higher-order correlations. The results identify the most important parameters for describing nuclear saturation and help prioritize efforts for uncertainty reduction of theoretical predictions. The achieved acceleration opens up an array of computational statistics analyses of the underlying description of the strong nuclear interaction in nuclei across the Segrè chart.

DOI: 10.1103/PhysRevLett.123.252501

Introduction.—How do properties of atomic nuclei depend on the underlying interaction between protons and neutrons? Recent *ab initio* computations of nuclei [1–16] have revealed that observables such as binding energies, radii, spectra, and decay probabilities are very sensitive to the values of the low-energy constants (LECs) in chiral Hamiltonian models with two- and three-nucleon forces [17–19]. Certain interaction models work better than others, but only for selected types of observables and in limited regions of the Segrè chart. It is not clear why. The NNLO$_{\mathrm{sat}}$ interaction [20] reproduces experimental binding energies and charge radii for nuclei up to mass $A \sim 50$ [4,5,9,16], while the 1.8/2.0 (EM) interaction [21,22] reproduces binding energies and low-lying energy spectra up to mass $A \sim 100$ [4,7,8,10,12,15], and while the radii are underestimated.

To improve theoretical predictions requires rigorous uncertainty quantification and sensitivity analyses that are grounded in the description of the underlying nuclear Hamiltonian. Unfortunately, the number of model samples required for statistical computing increases exponentially with the number of uncertain LECs. A global sensitivity analysis of the ground-state energy and charge radius ^{16}O, based on a realistic next-to-next-to-leading-order (NNLO) chiral Hamiltonian with 16 LECs, requires more than 10^6 model evaluations. Similar numbers can be expected for a Markov chain Monte Carlo sampling of Bayesian marginalization end evidence integrals [23–25]. Clearly, this is not feasible given the computational cost of existing state-of-the-art *ab initio* many-body methods applied to medium-mass and heavy nuclei.

In this Letter, we solve this problem by utilizing eigenvector continuation [26] to develop a subspace-projected coupled-cluster (SPCC) method as a fast and accurate approximation to the corresponding full-space CC method [27–33]. The SPCC method generalizes the eigenvector-continuation formalism in Ref. [34] to non-Hermitian problems and enables accelerated computation of nuclear observables across the Segrè chart for any target value $\vec{\alpha}_{\odot}$ of the LECs in the underlying Hamiltonian. See Fig. 1 for a demonstration of the SPCC method applied to ^{16}O and the variation of a single LEC (details are given below). We will use SPCC to analyze the description of the ^{16}O ground-state energy and charge radius across a large domain of relevant LECs. This way we can for the first time clearly identify the LECs that have the biggest impact on binding energy and radius predictions, which in turn impacts saturation properties of nuclear matter [8,35,36].

Method.—Following Ref. [34], we start by representing the chiral Hamiltonian at NNLO $H(\vec{\alpha})$ as a linear combination with respect to all of the LECs $\vec{\alpha}$; i.e., $H(\vec{\alpha}) = \sum_{i=0}^{N_{\mathrm{LECs}}=16} \alpha_i h_i$, with the zeroth term given by $h_0 = t_{\mathrm{kin}} + V_0$ and $\alpha_0 = 1$. Here t_{kin} is the intrinsic kinetic energy, and V_0 denotes a constant potential contribution that does not depend on any of the considered LECs—for example, the one-pion exchange interaction, the leading two-pion

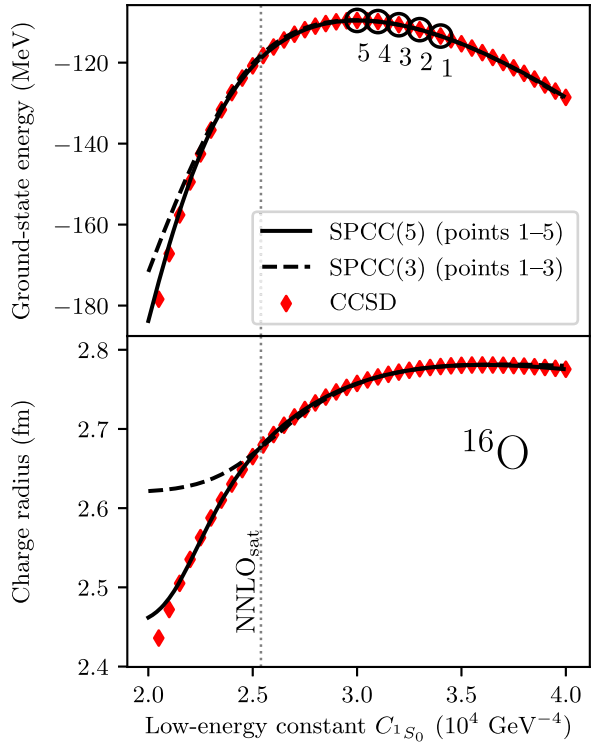

FIG. 1. SPCC results for ^{16}O, using three or five subspace vectors, for different values of the LEC $C_{^1S_0}$. The red diamonds indicate exact CC calculations at the singles and doubles level (CCSD). The NNLO$_{\rm sat}$ point is indicated with a dashed vertical line.

exchange, and terms proportional to the pion and nucleon masses. The analytical form of the NNLO Hamiltonian is identical to the one of NNLO$_{\rm sat}$ [20], including the regularization scheme, which means that, for a particular value $\vec{\alpha} = \vec{\alpha}_\star$, the Hamiltonian $H(\vec{\alpha}_\star)$ will reproduce the binding energy and radius predictions of NNLO$_{\rm sat}$. The SPCC Hamiltonian for a target value $\vec{\alpha} = \vec{\alpha}_\odot$ is constructed by projecting $H(\vec{\alpha}_\odot)$ onto the subspace spanned by CC wave functions obtained at $N_{\rm sub}$ different values for $\vec{\alpha}$. SPCC is a controlled approximation to the full-space CC method, and it allows for rapid and accurate solutions to the many-nucleon problem necessary for statistical computing. In this Letter, we use the CC method in the singles and doubles (CCSD) approximation.

The workhorse of the CC method is the similarity transformed Hamiltonian $\bar{H}(\vec{\alpha}) = e^{-T(\vec{\alpha})} H(\vec{\alpha}) e^{T(\vec{\alpha})}$, where in the CCSD approximation the cluster operator is truncated at one-particle–one-hole and two-particle–two-hole excitations, i.e., $T(\vec{\alpha}) = T_1(\vec{\alpha}) + T_2(\vec{\alpha})$. For clarity, we have indicated the implicit dependence on $\vec{\alpha}$. The CCSD similarity transformation is nonunitary and renders $\bar{H}(\vec{\alpha})$ non-Hermitian, and we thus introduce $N_{\rm sub}$ biorthogonal left and right CC ground states,

$$\langle\tilde{\Psi}| = \langle\Phi_0|[1 + \Lambda(\vec{\alpha})]e^{-T(\vec{\alpha})}, \qquad |\Psi\rangle = e^{T(\vec{\alpha})}|\Phi_0\rangle. \tag{1}$$

Here $\Lambda(\vec{\alpha}) = \Lambda_1(\vec{\alpha}) + \Lambda_2(\vec{\alpha})$ is a linear expansion in one-particle–one-hole and two-particle–two-hole deexcitation operators, and we have biorthonormality according to $\langle\tilde{\Psi}|\Psi\rangle = 1$. For notational simplicity, we will from here on omit the explicit $\vec{\alpha}$ dependence in the (de)excitation operators and set $T(\vec{\alpha}) = T$ and $\Lambda(\vec{\alpha}) = \Lambda$, respectively. The reference state $|\Phi_0\rangle$ is built from harmonic oscillator single-particle states, and we solve the CCSD equations in a model space comprising 11 major oscillator shells with a frequency $\hbar\Omega = 16$ MeV. The matrix elements of the three-nucleon interaction that enters the Hamiltonian are truncated by the energy cut $E_{3\,\rm max} \leq 14$. The CCSD result for ^{16}O with NNLO$_{\rm sat}$ in this model space is -118.76 MeV, which is within 1 MeV of the converged CCSD value using a Hartree-Fock basis.

Using the $N_{\rm sub}$ different CCSD ground-state vectors in Eq. (1), the matrix elements of the target Hamiltonian in the subspace and the corresponding norm matrix are given by

$$\begin{aligned}\langle\tilde{\Psi}'|H(\vec{\alpha}_\odot)|\Psi\rangle &= \langle\Phi_0|(1+\Lambda')e^{-T'}H(\vec{\alpha}_\odot)e^{T}|\Phi_0\rangle \\ &= \langle\Phi_0|(1+\Lambda')e^{X}\bar{H}(\vec{\alpha}_\odot)|\Phi_0\rangle, \end{aligned}\tag{2}$$

$$\langle\tilde{\Psi}'|\Psi\rangle = \langle\Phi_0|(1+\Lambda')e^{X}|\Phi_0\rangle, \tag{3}$$

respectively. Here we also introduced $e^X = e^{-T'+T}$, and $\bar{H}(\vec{\alpha}_\odot)$ is the similarity transformed target Hamiltonian. The left ground state $\langle\tilde{\Psi}'| = \langle\Phi_0|(1+\Lambda')e^{-T'}$ is obtained from $H(\vec{\alpha}')$, and the right ground state $e^T|\Phi_0\rangle$ is obtained from $H(\vec{\alpha})$. We can now solve the generalized non-Hermitian $N_{\rm sub} \times N_{\rm sub}$ eigenvalue problem for the SPCC target Hamiltonian to obtain the ground-state energy and wave function in the subspace. With the SPCC wave function, we can also calculate the expectation value of any subspace-projected operator with matrix elements $\langle\tilde{\Psi}'|O|\Psi\rangle$. Equations (2) and (3) can be evaluated using Wick's theorem, and closed form algebraic expressions are given in the Supplemental Material [37]. Note that in general the reference states for the $N_{\rm sub}$ different subspace CC wave functions in Eq. (1) are nonorthogonal. This is a nontrivial case and would require the generalized Wick's theorem [38,39] in order to evaluate the matrix elements of the SPCC Hamiltonian and the norm matrix.

Results.—The SPCC predictions for the energy and charge radius in ^{16}O as a function of the LEC $C_{^1S_0}$ in the Hamiltonian are shown in Fig. 1. Using $N_{\rm sub} = 5$ exact CCSD ground-state vectors, from a small region of $C_{^1S_0}$ values, points 1–5 in Fig. 1, the SPCC method extrapolates to the exact CCSD results across a large $C_{^1S_0}$ range. With $N_{\rm sub} = 3$ CCSD vectors, points 1–3 in Fig. 1, the radius extrapolation deteriorates far away from the exact solutions, while the energy predictions remain more accurate.

We now move to the challenging case where all 16 LECs at NNLO can vary. In the following, we analyze two SPCC Hamiltonians based on $N_{\rm sub} = 64$ and $N_{\rm sub} = 128$ CCSD

ground-state vectors, referred to as SPCC(64) and SPCC(128), respectively. The ground-state vectors are obtained at N_{sub} points in a domain of LEC values that surrounds the nominal LEC values of NNLO_{sat} within $\pm 20\%$ relative variation. This domain spans a rather large interval of ground-state energies and charge radii in ^{16}O. The three-nucleon contact LEC $c_E \approx 0.0395$ in NNLO_{sat} is small compared to the values of the remaining 15 LECs; we therefore scaled c_E with a factor of 20. In accordance with observation, we also constrained the leading-order isospin-breaking $^1S_0$ LECs ($\tilde{C}$) to exhibit small isospin breaking. We draw N_{sub} values for $\vec{\alpha}$ using a space-filling Latin hypercube design and solve for the exact CCSD wave function at each point. We have verified that the SPCC(64) and SPCC(128) Hamiltonians reproduce the energies and radii of the exact CCSD calculations for all N_{sub} choices of $\vec{\alpha}$.

Figure 2 shows the cross validation with respect to an additional set of 200 randomly drawn exact CCSD calculations in the same 20% domain. From the cross validation, we extract a root-mean-square error (RMSE) of SPCC(64): 4 MeV and 0.04 fm for the ground-state energy and charge radius, respectively. With SPCC(128), the RMSE values are 3 MeV and 0.02 fm. Using more subspace vectors gives better predictions. The present results are within the expected accuracy of CCSD. The nonhermiticity of the CCSD equations yields SPCC Hamiltonians that do not obey a variational bound with respect to the exact CCSD calculations. From Fig. 2, we see that this is a minute effect.

We use SPCC(64) and global sensitivity analysis (GSA) to analyze how the *ab initio* predictions for the energy and charge radius in ^{16}O explicitly depend on the LECs in the NNLO nuclear interaction. GSA is a very powerful, although computationally demanding, method for learning how much each unknown model parameter contributes to the uncertainty in a model prediction [40], as opposed to an uncertainty analysis, which addresses the question of how uncertain the prediction itself is. With SPCC, we can carry out the large amount of model evaluations that is required to extract statistically significant GSA results. In the following, we treat the ground-state energy or radius of ^{16}O as an output $Y = f(\vec{\alpha})$ of a model f, given here by the SPCC(64) Hamiltonian and its eigendecomposition. In the GSA, we decompose the total variance $\text{Var}[Y]$ as

$$\text{Var}[Y] = \sum_{i=1}^{N_{\text{LECs}}} V_i + \sum_{i<j}^{N_{\text{LECs}}} V_{ij} + \cdots, \tag{4}$$

where the partial variances are given by

$$\begin{aligned} V_i &= \text{Var}[E_{\vec{\alpha}\sim(\alpha_i)}[Y|\alpha_i]], \\ V_{ij} &= \text{Var}[E_{\vec{\alpha}\sim(\alpha_i,\alpha_j)}[Y|\alpha_i,\alpha_j]] - V_i - V_j, \end{aligned} \tag{5}$$

where $\text{Var}[E_{\vec{\alpha}\sim(\alpha_i)}[Y|\alpha_i]]$ denotes the variance of the conditional expectation of Y, and $\vec{\alpha} \sim (\alpha_i)$ denotes the set of all

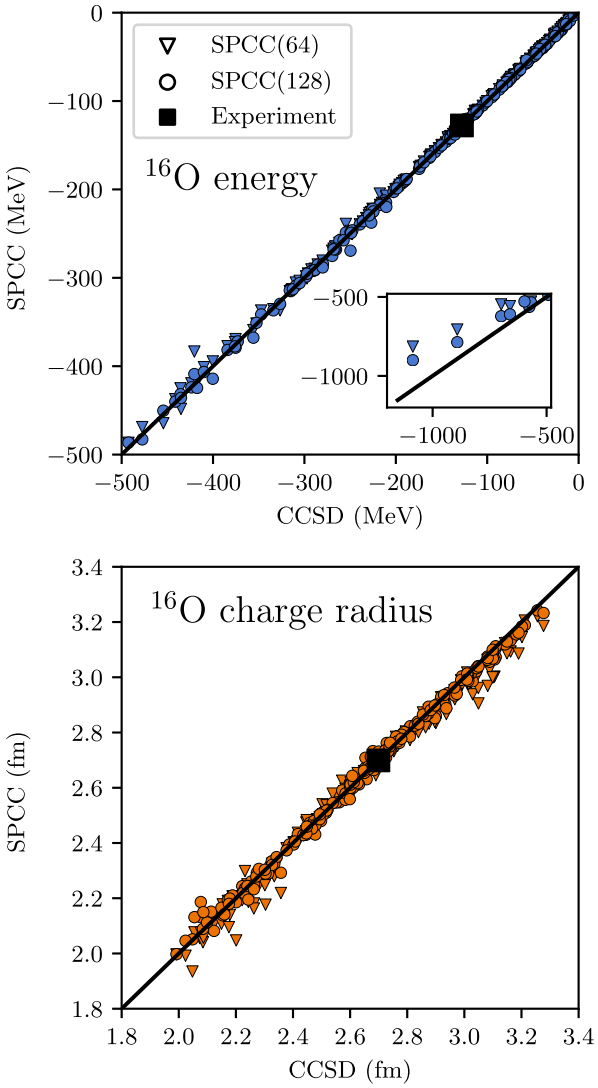

FIG. 2. Cross validation of SPCC(64) and SPCC(128) for (top panel) the ground-state energy and (bottom panel) charge radius using 200 exact CCSD calculations. (Inset) Energy predictions below −500 MeV. Only radii for negative-energy states shallower than −500 MeV are included.

LECs excluding α_i, and correspondingly for the second-order term. The variance integrals are evaluated using quasi–Monte Carlo (MC) sampling, and we extract a 95% confidence interval of the final result via bootstrap with 100 resamples [41]. The first- and second-order sensitivity indices are defined as

$$S_i = \frac{V_i}{\text{Var}[Y]}, \qquad S_{ij} = \frac{V_{ij}}{\text{Var}[Y]}. \tag{6}$$

The first-order sensitivity, S_i, is often referred to as the main effect. It apportions the total variance in the model output to an individual model parameter α_i. The higher-order indices, e.g., S_{ij}, apportion the variance in the model output to the combination of parameters α_i

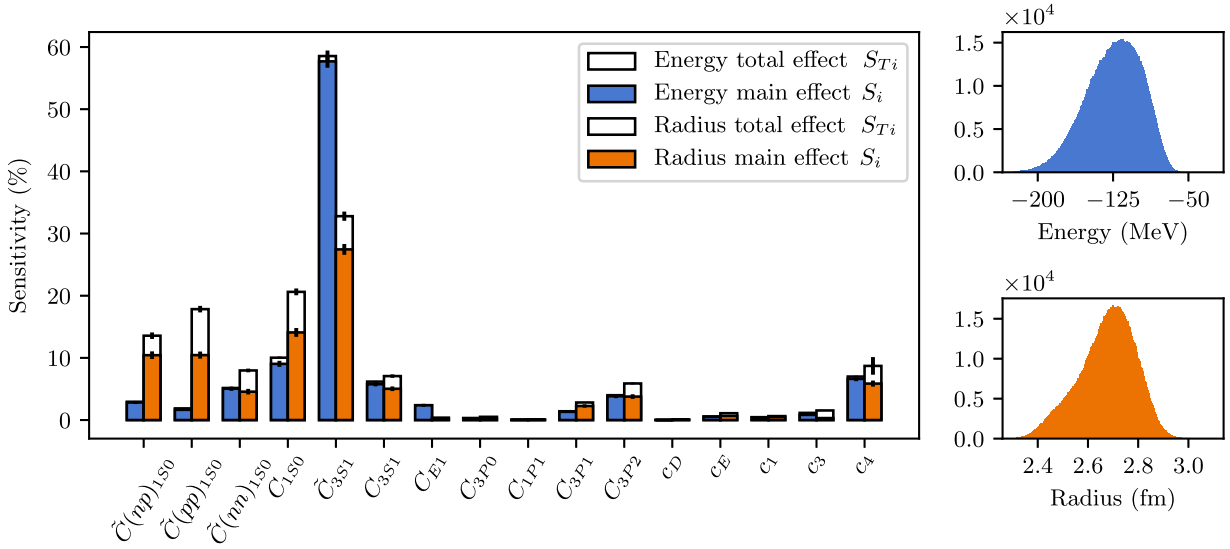

FIG. 3. (Left panel) Main and total effects (in %) for the ground-state energy (left bar) and charge radius (right bar) in ^{16}O, grouped per LEC. The main and total effects were computed from $(16+1)\times 2^{16} = 1\,114\,112$ quasi-MC evaluations of the SPCC(64) Hamiltonian. The vertical lines on each bar indicate bootstrapped 95% confidence intervals. A larger sensitivity value implies that the corresponding LEC is more critical for explaining the variance in model output. (Right panels) Histograms of (top panel) the ground-state energy and (bottom panel) charge radius from which the total variances are decomposed.

and α_j. The number of higher-order indices grow exponentially with the number of parameters in the model. Fortunately, it is possible to compute the sum of all sensitivity indices for each α_i, i.e., $S_{Ti} = S_i + S_{ij} + S_{ijk} + \cdots$. This is referred to as the total effect, and it quantifies the total sensitivity of $\mathrm{Var}[Y]$ to parameter α_i, including all of its higher-order parameter combinations [42]. We always have $S_{Ti} \geq S_i$ and equality for purely additive models. In this analysis, we do not calibrate the model to reproduce data. We study the behavior and response of the model itself, and we assume all LECs to be independent of each other and uniformly distributed. In future studies, one could draw LECs from a Bayesian posterior distribution.

Figure 3 shows the results from the GSA of the ^{16}O energy and radius using a SPCC(64) chiral NNLO Hamiltonian. To limit the model response of the energy and radius to a physically reasonable interval, we sample a LEC domain corresponding to 10% variation around the $\mathrm{NNLO_{sat}}$ values only. The LEC c_E is still scaled with a factor of 20. The MC sample size required for carrying out a reliable GSA depends on (i) the complexity of the model, and (ii) the number of parameters in the model. We have to use $(16+1)\times 2^{16} = 1\,114\,112$ quasi-MC samples to extract statistically significant main and total effects of the energy and radius for all LECs. With SPCC(64), this took about one hour on a standard laptop computer, while an equivalent set of exact CCSD computations would require 20 years. We find that 58(1)% of the variance in the energy can be attributed to the leading-order LEC $\tilde{C}_{^3S_1}$ and that all main and total effects are nearly identical, which signals that the energy is nearly additive in all LECs. We would like to point out that $\tilde{C}_{^3S_1}$ is directly proportional to the deuteron binding energy. However, to calibrate realistic nuclear interactions requires additional data, partly from heavier-mass nuclei; see, e.g., Ref. [20]. For the radius, the main effects are distributed across several LECs, and they differ from the total effects. Indeed, second-order correlations between the LECs are responsible for almost 14% of the variance in the radius. This result also reflects the challenge, and importance, of optimizing chiral NNLO Hamiltonians to reproduce radii of medium-mass atomic nuclei and, consequently, saturation properties of nuclear matter. Our analysis also reveals that the energy and radius of ^{16}O are not sensitive to the short-range parts of the three-nucleon interaction in this domain. Of the long-range πN LECs, $c_{1,3,4}$, only c_4 exhibits a non-negligible main effect for the energy and radius. This LEC contributes to the tensor force in the nucleon-nucleon interaction. As expected, only P-wave LECs with large spin weights contribute to the ^{16}O wave function. There also seems to be a larger sensitivity of the radius to the isospin-breaking terms in the interaction. Constraining the πN LECs to within the limits of the recent Roy-Steiner analysis [43] does not alter the sensitivity pattern or our conclusions. The GSA results guide future uncertainty reduction efforts for specific observables by identifying noninfluential LECs, which is also useful for, e.g., calibration. The SPCC method will significantly leverage statistical computation for analyzing correlations between different observables in different nuclei across the Segrè chart.

Summary and outlook.—We have developed the SPCC method for evaluating nuclear observables at different values of the LECs in chiral Hamiltonians at unprecedented speed. With a modest number of subspace vectors, $N_{\mathrm{sub}} = 64$, we reached 1% accuracy relative to exact CCSD solutions in ^{16}O. CC can also generate subspace vectors for heavier nuclei, and according to the theoretical underpinnings of eigenvector vector continuation, smooth changes of the wave function should mostly live in a low-dimensional manifold. Therefore, we expect the SPCC method to scale well with larger A. From a GSA, we conclude that the variance of the ground-state energy in ^{16}O is additive in all LECs of the NNLO chiral Hamiltonian, and that the charge radius depends sensitively on the combination of several LECs. The SPCC method enables a sophisticated statistical computation [44–47] in *ab initio* nuclear theory to reveal which new data would best reduce the uncertainty in Hamiltonian models and for understanding how properties of atomic nuclei depend on the underlying interaction between protons and neutrons. The stability of ^{16}O with respect to breakup into ^{4}He clusters is a relevant example [35,48–50]. The SPCC method also enables straightforward computation of derivatives with respect to the LECs using, e.g., algorithmic differentiation. SPCC Hamiltonians occupy very little disk space, and they can easily be shared within the nuclear community. SPCC matrix elements for ^{16}O are available from the authors

We thank Michael Grosskopf, Sebastian König, Dean Lee, Titus Morris, and Thomas Papenbrock for the fruitful discussions. G. H. acknowledges the hospitality of Chalmers University of Technology, where most of this work was carried out. This result is part of a project that has received funding from the European Research Council (ERC) under the European Union's Horizon 2020 research and innovation programme (Grant agreement No. 758027), the Office of Nuclear Physics, U.S. Department of Energy, under Grant No. desc0018223 (NUCLEI SciDAC-4 Collaboration), and by Field Work Proposal No. ERKBP72 at Oak Ridge National Laboratory (ORNL). Computer time was provided by the Innovative and Novel Computational Impact on Theory and Experiment (INCITE) program. This research used the resources of the Oak Ridge Leadership Computing Facility, located at ORNL, which is supported by the Office of Science of the Department of Energy under Contract No. DE-AC05-00OR22725.

[1] H. Hergert, S. K. Bogner, T. D. Morris, S. Binder, A. Calci, J. Langhammer, and R. Roth, *Ab initio* multireference in-medium similarity renormalization group calculations of even calcium and nickel isotopes, Phys. Rev. C **90**, 041302(R) (2014).

[2] S. Elhatisari, D. Lee, G. Rupak, E. Epelbaum, H. Krebs, T. A. Lähde, T. Luu, and U.-G. Meißner, *Ab initio* alpha-alpha scattering, Nature (London) **528**, 111 (2015).

[3] M. Rosenbusch *et al.*, Probing the $n = 32$ Shell Closure below the Magic Proton Number $z = 20$: Mass Measurements of the Exotic Isotopes ^{52,53}K, Phys. Rev. Lett. **114**, 202501 (2015).

[4] G. Hagen, A. Ekström, C. Forssén, G. R. Jansen, W. Nazarewicz, T. Papenbrock, K. A. Wendt, S. Bacca, N. Barnea, B. Carlsson, C. Drischler, K. Hebeler, M. Hjorth-Jensen, M. Miorelli, G. Orlandini, A. Schwenk, and J. Simonis, Neutron and weak-charge distributions of the ^{48}Ca nucleus, Nat. Phys. **12**, 186 (2016).

[5] R. F. Garcia Ruiz *et al.*, Unexpectedly large charge radii of neutron-rich calcium isotopes, Nat. Phys. **12**, 594 (2016).

[6] V. Lapoux, V. Somà, C. Barbieri, H. Hergert, J. D. Holt, and S. R. Stroberg, Radii and Binding Energies in Oxygen Isotopes: A Challenge for Nuclear Forces, Phys. Rev. Lett. **117**, 052501 (2016).

[7] G. Hagen, G. R. Jansen, and T. Papenbrock, Structure of ^{78}Ni from First-Principles Computations, Phys. Rev. Lett. **117**, 172501 (2016).

[8] J. Simonis, S. R. Stroberg, K. Hebeler, J. D. Holt, and A. Schwenk, Saturation with chiral interactions and consequences for finite nuclei, Phys. Rev. C **96**, 014303 (2017).

[9] T. Duguet, V. Somà, S. Lecluse, C. Barbieri, and P. Navrátil, *Ab initio* calculation of the potential bubble nucleus ^{34}Si, Phys. Rev. C **95**, 034319 (2017).

[10] T. D. Morris, J. Simonis, S. R. Stroberg, C. Stumpf, G. Hagen, J. D. Holt, G. R. Jansen, T. Papenbrock, R. Roth, and A. Schwenk, Structure of the Lightest Tin Isotopes, Phys. Rev. Lett. **120**, 152503 (2018).

[11] B.-N. Lu, N. Li, S. Elhatisari, D. Lee, E. Epelbaum, and U.-G. Meiner, Essential elements for nuclear binding, Phys. Lett. B **797**, 134863 (2019).

[12] H. N. Liu *et al.*, How Robust is the $n = 34$ Subshell Closure? First Spectroscopy of ^{52}Ar, Phys. Rev. Lett. **122**, 072502 (2019).

[13] R Taniuchi *et al.*, ^{78}Ni revealed as a doubly magic stronghold against nuclear deformation, Nature (London) **569**, 53 (2019).

[14] P. Gysbers, G. Hagen, J. D. Holt, G. R. Jansen, T. D. Morris, P. Navrátil, T. Papenbrock, S. Quaglioni, A. Schwenk, S. R. Stroberg, and K. A. Wendt, Discrepancy between experimental and theoretical β-decay rates resolved from first principles, Nat. Phys. **15**, 428 (2019).

[15] J. D. Holt, S. R. Stroberg, A. Schwenk, and J. Simonis, *Ab initio* limits of atomic nuclei, arXiv:1905.10475.

[16] V. Somà, P. Navrátil, F. Raimondi, C. Barbieri, and T. Duguet, Novel chiral Hamiltonian and observables in light and medium-mass nuclei, arXiv:1907.09790.

[17] U. Van Kolck, Effective field theory of nuclear forces, Prog. Part. Nucl. Phys. **43**, 337 (1999).

[18] E. Epelbaum, H.-W. Hammer, and U.-G. Meißner, Modern theory of nuclear forces, Rev. Mod. Phys. **81**, 1773 (2009).

[19] R. Machleidt and D. R. Entem, Chiral effective field theory and nuclear forces, Phys. Rep. **503**, 1 (2011).
[20] A. Ekström, G. R. Jansen, K. A. Wendt, G. Hagen, T. Papenbrock, B. D. Carlsson, C. Forssén, M. Hjorth-Jensen, P. Navrátil, and W. Nazarewicz, Accurate nuclear radii and binding energies from a chiral interaction, Phys. Rev. C **91**, 051301(R) (2015).
[21] A. Nogga, S. K. Bogner, and A. Schwenk, Low-momentum interaction in few-nucleon systems, Phys. Rev. C **70**, 061002(R) (2004).
[22] K. Hebeler, S. K. Bogner, R. J. Furnstahl, A. Nogga, and A. Schwenk, Improved nuclear matter calculations from chiral low-momentum interactions, Phys. Rev. C **83**, 031301(R) (2011).
[23] M. R. Schindler and D. R. Phillips, Bayesian methods for parameter estimation in effective field theories, Ann. Phys. (Amsterdam) **324**, 682 (2009).
[24] S. Wesolowski, N. Klco, R. J. Furnstahl, D. R. Phillips, and A. Thapaliya, Bayesian parameter estimation for effective field theories, J. Phys. G **43**, 074001 (2016).
[25] S. Wesolowski, R. J. Furnstahl, J. A. Melendez, and D. R. Phillips, Exploring Bayesian parameter estimation for chiral effective field theory using nucleon-nucleon phase shifts, J. Phys. G **46**, 045102 (2019).
[26] D. Frame, R. He, I. Ipsen, D. Lee, D. Lee, and E. Rrapaj, Eigenvector Continuation with Subspace Learning, Phys. Rev. Lett. **121**, 032501 (2018).
[27] F. Coester, Bound states of a many-particle system, Nucl. Phys. **7**, 421 (1958).
[28] F. Coester and H. Kümmel, Short-range correlations in nuclear wave functions, Nucl. Phys. **17**, 477 (1960).
[29] H. Kümmel, K. H. Lührmann, and J. G. Zabolitzky, Many-fermion theory in exp $S-$ (or coupled cluster) form, Phys. Rep. **36**, 1 (1978).
[30] B. Mihaila and J. H. Heisenberg, Microscopic Calculation of the Inclusive Electron Scattering Structure Function in ^{16}O, Phys. Rev. Lett. **84**, 1403 (2000).
[31] D. J. Dean and M. Hjorth-Jensen, Coupled-cluster approach to nuclear physics, Phys. Rev. C **69**, 054320 (2004).
[32] R. J. Bartlett and M. Musiał, Coupled-cluster theory in quantum chemistry, Rev. Mod. Phys. **79**, 291 (2007).
[33] G. Hagen, T. Papenbrock, M. Hjorth-Jensen, and D. J. Dean, Coupled-cluster computations of atomic nuclei, Rep. Prog. Phys. **77**, 096302 (2014).
[34] S. König, A. Ekström, K. Hebeler, D. Lee, and A. Schwenk, Eigenvector continuation as an efficient and accurate emulator for uncertainty quantification, arXiv:1909.08446.
[35] A. Ekström, G. Hagen, T. D. Morris, T. Papenbrock, and P. D. Schwartz, Delta isobars and nuclear saturation, Phys. Rev. C **97**, 024332 (2018).
[36] C. Drischler, K. Hebeler, and A. Schwenk, Chiral Interactions Up to Next-to-Next-to-Next-to-Leading Order and Nuclear Saturation, Phys. Rev. Lett. **122**, 042501 (2019).
[37] See Supplemental Material at http://link.aps.org/supplemental/10.1103/PhysRevLett.123.252501 for the algebraic expressions of the subspace projected CCSD Hamiltonian and norm matrix.
[38] C. A. Jiménez-Hoyos, R. Rodríguez-Guzmán, and G. E. Scuseria, *n*-electron Slater determinants from nonunitary canonical transformations of fermion operators, Phys. Rev. A **86**, 052102 (2012).
[39] F. Plasser, M. Ruckenbauer, S. Mai, M. Oppel, P. Marquetand, and L. Gonzlez, Efficient and flexible computation of many-electron wave function overlaps, J. Chem. Theory Comput. **12**, 1207 (2016).
[40] I. M. Sobol, Global sensitivity indices for nonlinear mathematical models and their Monte Carlo estimates, Math. Comput. Simul. **55**, 271 (2001).
[41] A. Saltelli, P. Annoni, I. Azzini, F. Campolongo, M. Ratto, and S. Tarantola, Variance based sensitivity analysis of model output. Design and estimator for the total sensitivity index, Comput. Phys. Commun. **181**, 259 (2010).
[42] T. Homma and A. Saltelli, Importance measures in global sensitivity analysis of nonlinear models, Reliability Engineering and System Safety **52**, 1 (1996).
[43] M. Hoferichter, J. Ruiz de Elvira, B. Kubis, and U.-G. Meißner, Matching Pion-Nucleon Roy-Steiner Equations to Chiral Perturbation Theory, Phys. Rev. Lett. **115**, 192301 (2015).
[44] A. Gelman, J. B. Carlin, H. S. Stern, D. B. Dunson, A. Vehtari, and D. B. Rubin, *Bayesian Data Analysis*, 3rd ed., Chapman and Hall/CRC Texts in Statistical Science Vol. 106 (Chapman and Hall, London, 2013).
[45] J. D. McDonnell, N. Schunck, D. Higdon, J. Sarich, S. M. Wild, and W. Nazarewicz, Uncertainty Quantification for Nuclear Density Functional Theory and Information Content of New Measurements, Phys. Rev. Lett. **114**, 122501 (2015).
[46] L. Neufcourt, Y. Cao, W. Nazarewicz, E. Olsen, and F. Viens, Neutron Drip Line in the Ca Region from Bayesian Model Averaging, Phys. Rev. Lett. **122**, 062502 (2019).
[47] I. Vernon, M. Goldstein, and R. G. Bower, Galaxy formation: A Bayesian uncertainty analysis, Bayesian Anal. **5**, 619 (2010).
[48] B. D. Carlsson, A. Ekström, C. Forssén, D. Fahlin Strömberg, G. R. Jansen, O. Lilja, M. Lindby, B. A. Mattsson, and K. A. Wendt, Uncertainty Analysis and Order-by-Order Optimization of Chiral Nuclear Interactions, Phys. Rev. X **6**, 011019 (2016).
[49] L. Contessi, A. Lovato, F. Pederiva, A. Roggero, J. Kirscher, and U. van Kolck, Ground-state properties of ^{4}He and ^{16}O extrapolated from lattice QCD with pionless EFT, Phys. Lett. B **772**, 839 (2017).
[50] A. Bansal, S. Binder, A. Ekström, G. Hagen, G. R. Jansen, and T. Papenbrock, Pion-less effective field theory for atomic nuclei and lattice nuclei, Phys. Rev. C **98**, 054301 (2018).